Scientific Reports

https://doi.org/10.1038/s41598-026-41436-z

Article in Press

Implementation of smart metasurfaces for the Sub-6 GHz 5G wireless systems: design, optimization, and its synthesis for enhancing antenna's performance

Received: 5 May 2025

Accepted: 19 February 2026

Published online: 25 February 2026

Cite this article as: Behera B.R., Paik H., Kumar J.A. *et al.* Implementation of smart metasurfaces for the Sub-6 GHz 5G wireless systems: design, optimization, and its synthesis for enhancing antenna's performance. *Sci Rep* (2026). https://doi.org/10.1038/s41598-026-41436-z

Bikash Ranjan Behera, Harikrishna Paik, J. Arun Kumar, Mohammed H. Alsharif, Sabri Saeed & Khalid Yahya

We are providing an unedited version of this manuscript to give early access to its findings. Before final publication, the manuscript will undergo further editing. Please note there may be errors present which affect the content, and all legal disclaimers apply.

If this paper is publishing under a Transparent Peer Review model then Peer Review reports will publish with the final article.

ARTICLE IN PRESS

© The Author(s) 2026. **Open Access** This article is licensed under a Creative Commons Attribution-NonCommercial-NoDerivatives 4.0 International License, which permits any non-commercial use, sharing, distribution and reproduction in any medium or format, as long as you give appropriate credit to the original author(s) and the source, provide a link to the Creative Commons licence, and indicate if you modified the licensed material. You do not have permission under this licence to share adapted material derived from this article or parts of it. The images or other third party material in this article are included in the article's Creative Commons licence, unless indicated otherwise in a credit line to the material. If material is not included in the article's Creative Commons licence and your intended use is not permitted by statutory regulation or exceeds the permitted use, you will need to obtain permission directly from the copyright holder. To view a copy of this licence, visit http://creativecommons.org/licenses/by-nc-nd/4.0/.

ARTICLE IN PRESS

Implementation of Smart Metasurfaces for the Sub-6 GHz 5G Wireless Systems: Design, Optimization, and its Synthesis for Enhancing Antenna's Performance

Bikash Ranjan Behera [1], Harikrishna Paik [1], J. Arun Kumar [1], Mohammed H. Alsharif [3,*], Sabri Saeed [4,*] and Khalid Yahya [5]

[1] Department of Electronics and Communication Engineering, Vel Tech Rangarajan Dr.Sagunthala R&D Institute of Science and Technology (Deemed-to-Be-University), Chennai, Tamil Nadu, India

[3] Department of AI Convergence Electronic Engineering, Sejong University, Seoul 05006, Korea

[4] Department of Networks and Cybersecurity, Aljanad University for Science and Technology, Taiz, Yemen

[5] Department of Electrical and Engineering, Faculty of Engineering and Architecture, Istanbul Gelisim Univer--sity, Istanbul, Turkey

bikashranjan.behera@gmail.com [1], pavan_paik2003@yahoo.co.in [2], conveytoarun87@gmail.com [3], malsharif @sejong.ac.kr [4], sabri.alshibany@just.edu.ye [5*], and hayahya@gelisim.edu.tr [6]

Corresponding Author: Mohammed H. Alsharif (malsharif@sejong.ac.kr); Sabri Saeed (sabri.alshibany@just.edu.ye)

ARTICLE IN PRESS

Abstract-A broadened polarization bandwidth with a high-gain SADEA-driven metasurface antenna at 5 GHz is investigated for the sub-6 GHz 5G wireless applications. At first, a $\lambda_o/4$ linearly polarized printed monopole antenna is considered. In the next step, a metallic strip that serves as a dynamic switching mechanism is used to short one of the parasitic conducting strips with a partial ground plane to get circular polarization (CP). To make it suitable for the RF energy harvesting application, a crucial part of sub-6 GHz 5G communication, the motive is to achieve broadened performance for antenna gain, impedance (10-dB BW), and axial bandwidths (3-dB BW). It is attained by placing the SADEA-tuned metasurface layer as a parasitic patch at the height of $0.02\lambda_o$, below the radiator. With the usage of the SADEA optimization method, the process of the metasurface layer is depicted as more effective in performance and less complex towards its execution. It is printed on FR-4 of $1.33\lambda_o \times 0.9\lambda_o \times 0.02\lambda_o$, which offers a measured 58.23% 10-dB BW, 26.39% 3-dB BW, CP gain ^{peak} > 5.9 dBic, antenna efficiency > 75%, with a front-to-back ratio > -20 dBic in the sub-6 GHz 5G bands, a potential candidate for the next-generation wireless communication, especially for the RF energy harvesting systems.

Keywords-Monopole Antenna, Circular Polarization, SADEA Optimization, Metasurfaces, Sub-6 GHz 5G Applications, RF Energy Harvesting.

1. Introduction

The wireless communication is rapidly progressing towards 5G & has significant expectations for data speeds, coverage, capacity, efficiency, connectivity, & latency [1, 2]. It is in comparison with a communication system that is in existence. By enhancing their capabilities, the RF front-ends play a pivotal role in the phenomena of building a next-generation communication system [3, 4]. This advancement is made possible by the expansion of the RF wireless system. When the current circumstances are taken into consideration, there is an immediate need for research that is focused

ARTICLE IN PRESS
toward the development of energy harnessing with the assistance of ambient signals & sub-6 GHz 5G. RF energy harvesting through the use of the EM spectrum has developed as a means of reducing costs with less periodic maintenance. It emerges as the result of the fact that low-power embedded devices are taken into consideration. So, reference is being made for the utilization of energy, where RF front-ends are considered to be a crucial component of the process; the reason for this is that it requires interaction with EM waves that are all around us [5, 6]. Using circular polarization (CP) to produce better signal matching is one way to measure its effectiveness in terms of better signal matching, as the first step is to make sure that the incoming signals from mobile communication bands are received accurately, irrespective of the direction in which the antenna is pointed. Their selection is of importance due to their low profile, simplicity to analyze, broad bandwidth, good radiation efficiency, desirable pattern, time domain utility, and sensitivity to the FCC emission limits, as its primary requirements [7-12]. Thus, a printed monopole was selected with the motive of improving capabilities through the designing of effective CP antennas in their desired operating bands [13].

As a consequence of this, there is a requirement for the single antenna element that possesses attributes, mostly the capability of CP. So, the techniques in the likes of vias [14] & metasurfaces (MTS) [15-28] are utilized in order to accomplish designing the CP antennas. On the other hand, when it comes to the requirements for an effective polarization system (high polarization bandwidth with a fractional bandwidth ratio of > 20%), one of the important requirements is to obtain the broadband CP. Because this particular kind of comparison was not specified in [14-28], as it continues to be a significant [29]. As this is especially true when it processes to the deployment of MTS layers that are not properly defined through the AI. The method that is SADEA [30] was used for the goal of optimizing parameters to enhance performances, taking into consideration a variety of requirements. The application of this method to the optimization of MTS is essential towards the CP antenna in terms of its augmentation, bandwidth, & gain. So, the broadband CP & broadside directional patterns were attained with the use of a metallic strip & incorporation of a SADEA-driven MTS layer as a parasitic patch. Following that, the analogy of CP has been proposed by means of the CEM, which is shown later. This article investigates the MTS-SADEA-inspired monopole antenna, offering performance while considering trade-offs, i.e., the broadened 3-dB bandwidth of > 20% and a CP gain $^{avg.}$ of > 5.25 dBic with an effective polarization in terms of the optimum front-to-back ratio for the sub-6 GHz 5G bands. In the remaining sections, information about the counterparts is well explained out, i.e., right from theoretical insights to experimental validation to its implementation from an application perspective.

ARTICLE IN PRESS

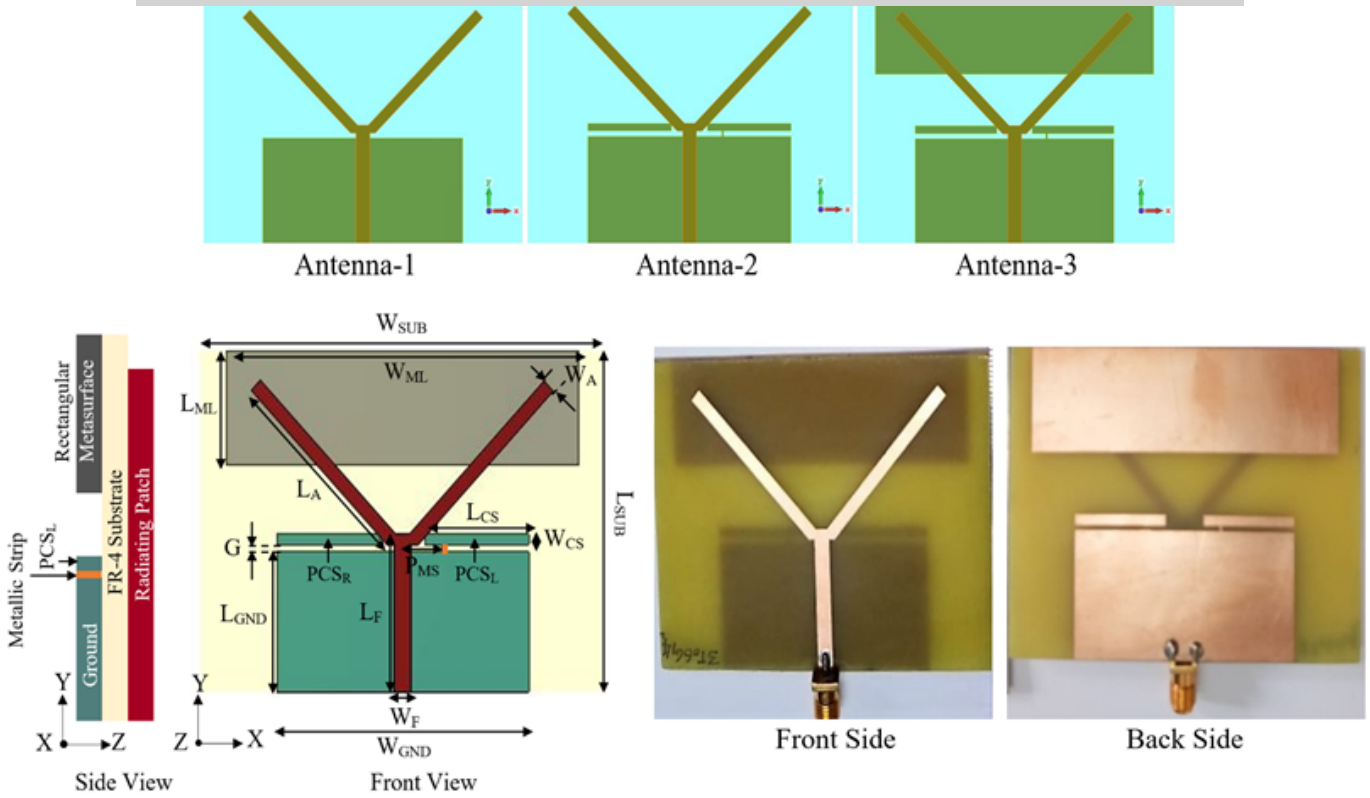

Figure 1. Evolution stages and the schematics of SADEA-tuned MTS antenna with its fabricated prototype.

2. Antenna Design and its Analysis

An illustration of the evolution stages & schematics of a Y-shaped MTS antenna printed on an FR-4 substrate is shown in Figure 1. In the designing procedure, the authors have extended the partial ground plane (PGP) by adding the conducting strips in order to address trade-offs (antenna-1 to antenna-2). So, these are separated from the upper faces of the PGPs by an offset of 1.16 mm, whose length is 21.6 mm and the width is 1.84 mm (antenna-1). When viewed from the application point of view, the interaction that takes place in between PGP and the conducting strip, PCS_L, is an essential factor in determining the CP attributes. Through the usage of a metallic strip (antenna-2), it is possible to establish communication by connecting PGP & PCS_L. Finally, the utilization of the SADEA-tuned MTS layer as a parasitic patch provides broadband CP traits in the form of a focused bi-directional pattern that possesses increased FBR and a 3 dB angular beamwidth of > 100° in the desired band of 3.5/5 GHz, a key part of the sub-6 GHz 5G wireless communication systems (i.e., antenna-3). Then, a structural parametric study of antenna-2 is pursued for various counterparts. All components of these printed antennas (i.e., antenna-3) must be optimized properly because surface currents render a significant role in generating their favorable radiation characteristics, maintaining good polarization bandwidth, and gain. As, when a full ground plane is used, considering the specified CP frequency range, 10-dB impedance bandwidth (10-dB BW) and 3-dB axial bandwidth (3-dB BW) diminish to an extent by affecting the attainment of trade-offs. As a result of this, it also alters the radiation pattern. Due to horizontal component dependency, the axial ratio is more sensitive to the ground plane width (W_{GND}) found during the parametric investigations. Prior, it is also sensitive to parasitic conducting strip length (L_{CS}), width (W_{CS}), & position (P_{MS}), where metallic strip is used to short the PGP and PCS_L, an extended geometric driven activity. The variation of L_{CS}, W_{CS}, and P_{MS} also affect the 10-dB BW and 3-dB BW, due to the consideration of an equal magnitude horizontal and vertical components with the phase-time difference, as illustrated in Figures 2(a)-(c), respectively.

ARTICLE IN PRESS

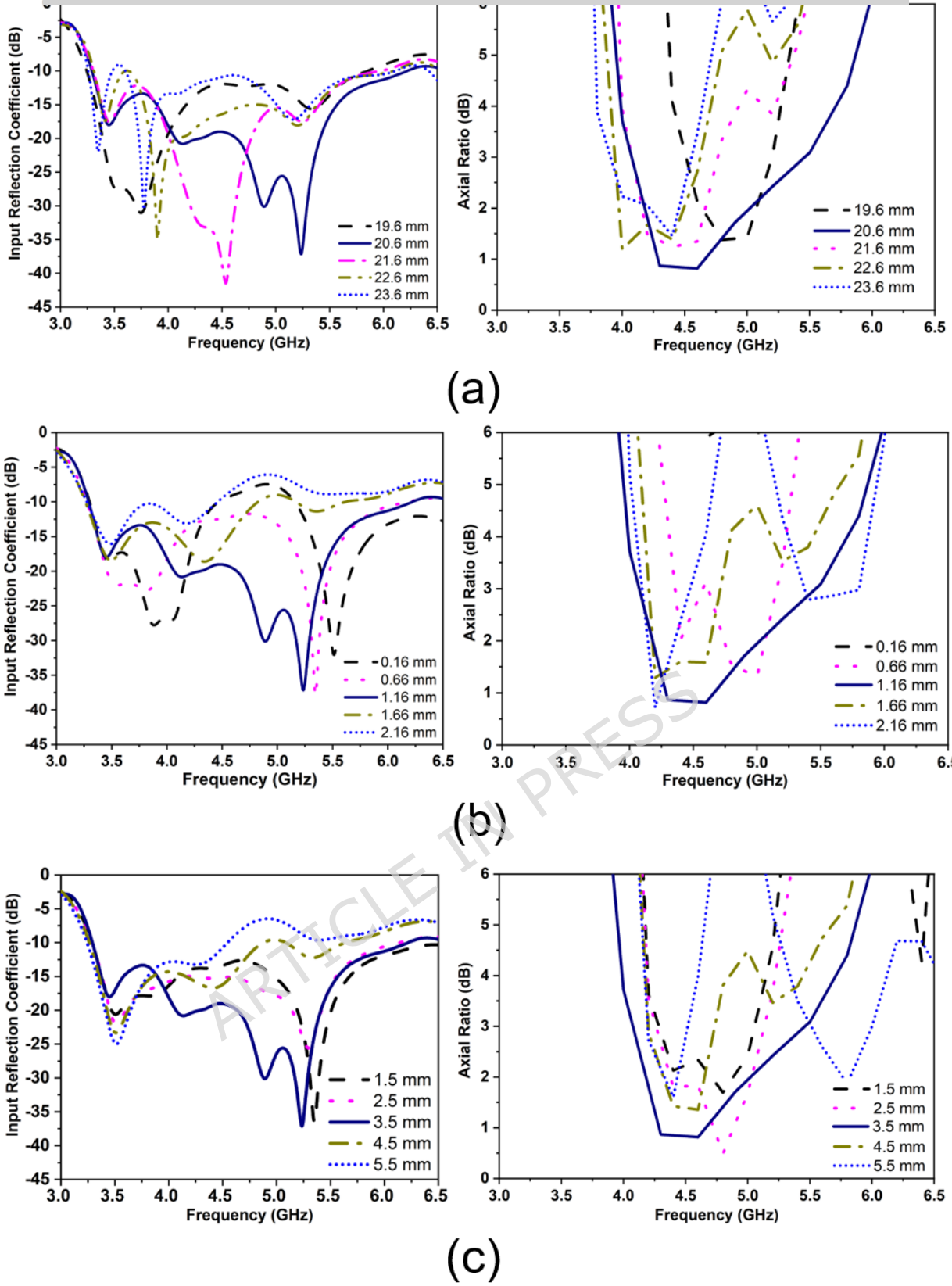

Figure 2. Parametric changes on 10-dB BW & 3-dB BW due to the variation in: (a) L_{CS}, (b) W_{CS}, and (c) P_{MS}.

Then, we proceed to elucidate on the method of incorporating SADEA-tuned MTS into the case of metasurface antenna for RF energy harvesting application. So, when the users make use of MATLAB Antenna Toolbox™, they are offered access to the wide variety of functions & applications that are utilized for the goal of creating, analyzing, & visualizing the RF ends. As a result of the component elements, i.e., MTS, a parasitic patch has been designed. So, the fact that it makes use of an EM solver enables it to compute final verifications, as MoM does. Through manual optimization, it is possible to optimize the proposed design in a most effective manner, but the attainment of trade-offs from an application perspective was still far from reach. Therefore, by using the fundamental concepts of AI, the SADEA approach [31] is brought into

ARTICLE IN PRESS

consideration. This method is used to optimize designs on the basis of a theoretical foundation that it is framed [30-32].

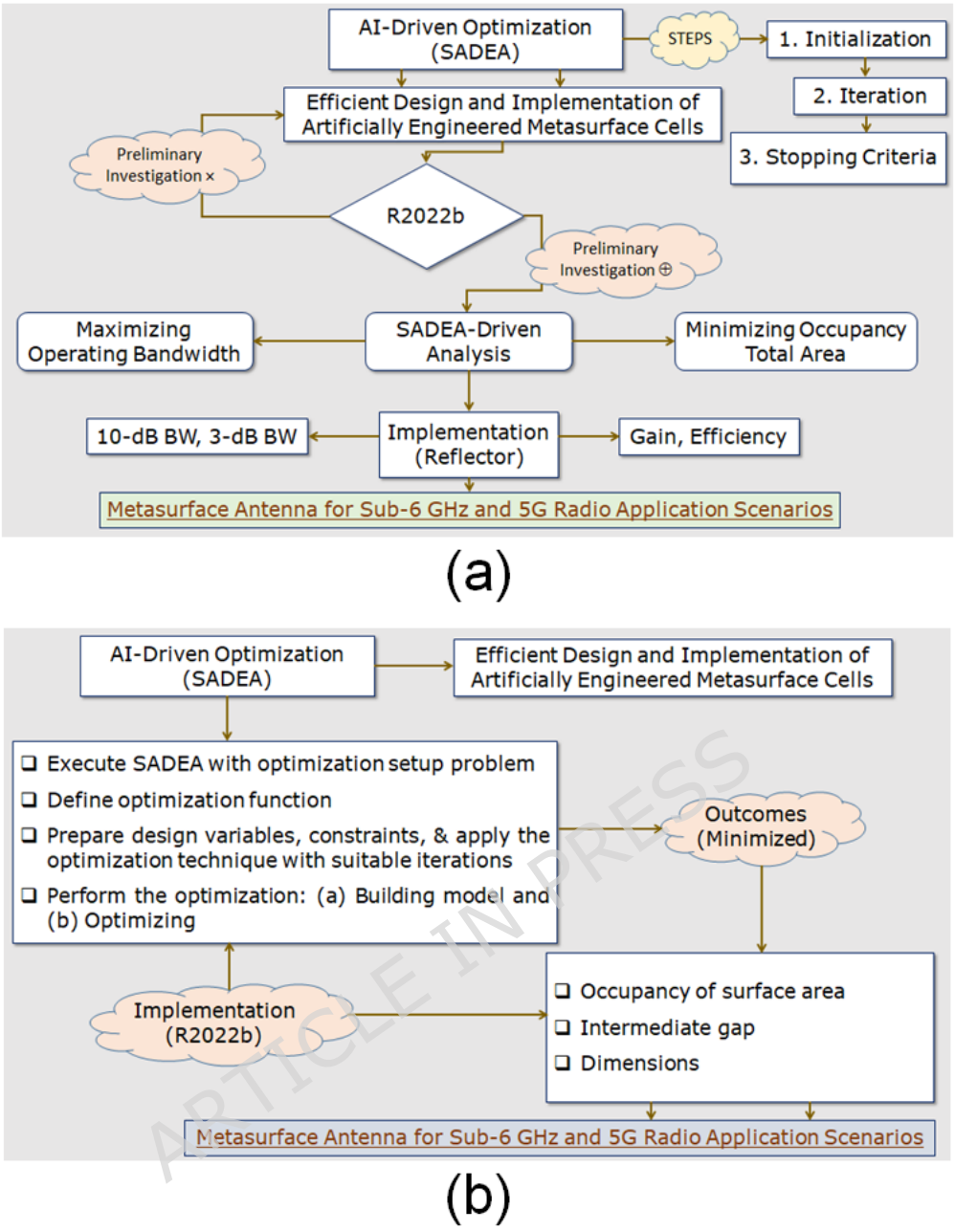

Figure 3. (a), (b) Concept, process, and its implementation of SADEA optimization method in antenna-3.

The process of global optimization, which is carried out with the assistance of SADEA, makes use of statistical learning methodologies in order to develop the surrogate model. Hence, in the context of the surrogate model-assisted optimization technique, it is of the utmost importance that the procedure followed to prepare surrogate modeling & its optimization should work together in a successful manner. This is because the surrogate model is the model that is being optimized, as SADEA has incorporated notions that were taken from an evolutionary search framework that takes surrogate models into consideration, as concepts were acquired from its evolution. A Gaussian process (GP) is applied in both the search engine that SADEA uses, which is known as differential evolution (DE), and the machine learning technique that is utilized for the same surrogate modeling [33]. Both of the technologies are referred to as DE. So, surrogate models estimate the goal functions—the actual antenna performance. These models are trained on a restricted set of design points assessed via the simulations. Hence, based on the design parameters, it estimates the performance factor of the antenna. Regarding the optimization of MTS

ARTICLE IN PRESS

acting as parasitic patch, it appears that the SADEA optimization method is used in rare circumstances when it comes to its optimizing. This process not only improves conventional DE but also provides antenna synthesis benefits; full-wave EM simulation is costly and relies on increasing complexity & time consumption. Hence, reducing the number of expensive assessments as the surrogate model significantly approximates the objective function. The following steps are taken into consideration during the entire AI-driven optimization process in the MATLAB platform:

- **Step-1: Initialization** – Create a population of potential solutions at first, each of which represents some different antenna design parameters with different characteristics.
- **Step-2: Surrogate Model Training** – A subset of evaluated solutions is used to train the surrogate as DE process moves on. Based on the values of its parameters, this model learns to forecast how antenna design parameters would function and impact the performance.
- **Step-3: Optimization Process** – The surrogate model is used to direct the algorithm. Instead of executing a full simulation for each design parameter, the model predicts their performance, which the algorithm then utilizes to select the best dimension for an execution before integrating it into the MTS structure.
- **Step-4: Updating Surrogate** – It is updated with recent dimensions after a sufficient number of iterations have been tested. So that it can get better over time and make the prediction accurate.
- **Step-5: Termination** – The process of optimization will continue until these stopping criteria are satisfied, which could be a predetermined number of iterative generations from the beginning/discovery of a solution that provides a good response. Hence, SADEA not only reduces the expensive simulations while keeping the methods' robustness to optimize the MTS design parameters given in Table 1 for the better outcomes.

ARTICLE IN PRESS

Table 1. Optimized dimensions of the SADEA-tuned MTS layer acting as a parasitic patch.

Parameters	Description	Range	SADEA (Antenna-3)
W_{ML}	Width of the MTS layer	60 mm - 80 mm	70 mm
L_{ML}	Length of the MTS layer	10 mm - 30 mm	20 mm
$(W_{SUB}-W_{ML})/2$	Width of the Intermediate Gap	0 mm - 10 mm	5 mm
$(L_{SUB}-L_{ML})/2$	Length of the Intermediate Gap	10 mm - 30 mm	20 mm

During the investigation in MATLAB platform, the advantages of faster optimization, improved convergence, less complexity, and better global search are observed, which makes it the optimization method for optimizing the MTS layer to the best of the authors' knowledge. In order to simplify the understanding, from the start to the end of the optimization, a comprehensive flow of the procedure that is involved and its implementation is presented in Figures 3(a) & (b). So, the purpose of the optimization is to bring improvements in the outcomes: (a) maximizing antenna's performance (antenna-3) and (b) limiting the region of occupation (ROO) for MTS. During this analysis a crucial observation is made: that the performance trade-offs from the perspective of the application are considered as a final stopping criterion, ensuring

ARTICLE IN PRESS

that the antenna's performance is maintained. For better results, the execution of the rectangular MTS as parasitic patch is carried out. It involves optimizing the (a) size of the patch and (b) intermediate gap from the two sides. Then, placed at a height of $0.02\lambda_o$ below antenna-3, without the concern of disturbing the overall size of antenna-3. The optimized dimension is shown in Table 1. As a result, the antenna's performance at the 5 GHz band was prolonged to a great extent, satisfying the performance trade-offs.

Continuing with our investigation, when compared to 2.35 dBic (antenna-2, w/o MTS layer), the CP gain $^{avg.}$ improves by the factor of 2.24, reaching 5.28 dBic. This suggests that the CP gain has increased to an extent. Further, the 10-dB BW of the MTS antenna increases by a factor of 3.36 times, from 0.9 GHz to 3.03 GHz, and the 3-dB BW increases by a factor of 5.0 times, from 0.29 GHz to 1.45 GHz (antenna-3, with MTS layer), compared with antenna-1. Both of the increments are attributed to the presence of SADEA-driven MTS layer as a parasitic patch. The improvement of both of them is of utmost importance. In light of the matter that the objective of the development is to achieve the trade-offs (antenna-3), the attainment of antenna performances is driven by geometric knowledge. MTS is proposed to concentrate radiation beams towards the quasi-TM30 modes (transformation of TM10 to TM30 modes) by applying FIT. This results in a more uniform distribution of the E-field, leading to an improvement in the impedance performance. It is the MTS that are the sources of high-order modes in terms of wavelength shown in Figure 4. So, a correlation between the lower Q-values & the enhancement of bandwidth can be established throughout the design stages. The reason for this is that the relationship between bandwidth and Q-factor is inversely proportional. Thus, there is a connection in between the physical properties of the MTS layer & the enhancement of antenna gains. Since the MTS layer can control the phase, amplitude, and polarization of the waves. Therefore, shaping the wave front allows them to guide the radiated energy in the more focused direction, improving the directivity of the antenna & so its gain. It is the only reason why the parasitic patch is termed as MTS, & to the best of the author's knowledge, this is the first time where the dimensions of MTS are optimized by using an AI-driven optimization method keeping at par with the performance trade-offs.

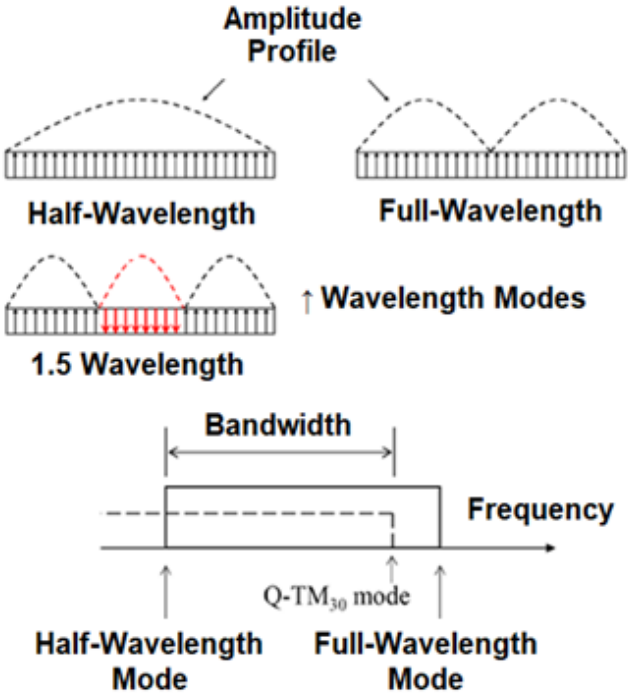

Figure 4. Transformation of half-wavelength to full-wavelength modes in antenna-3, where MTS is taken as a parasitic patch.

ARTICLE IN PRESS

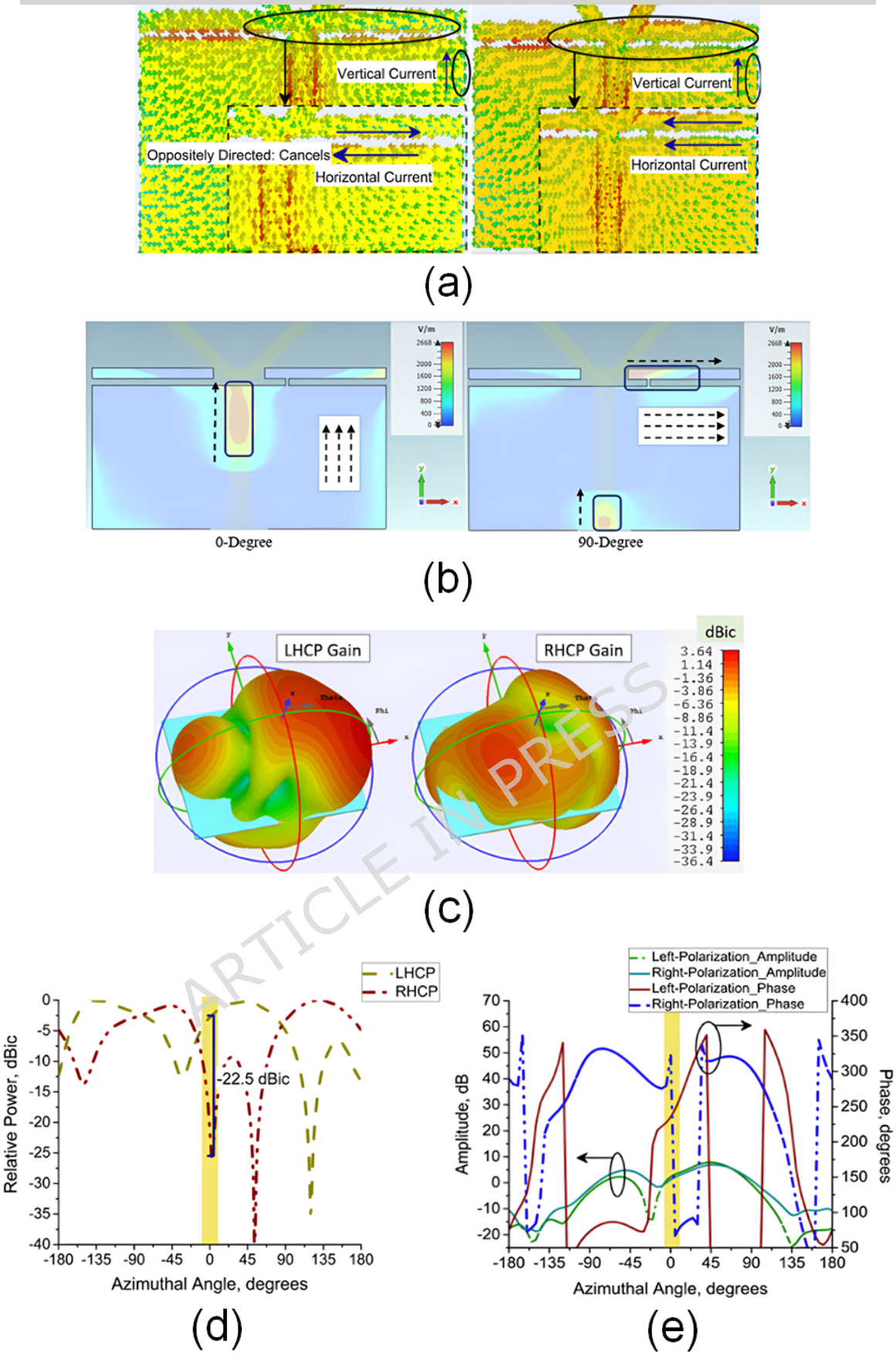

Figure 5. Understanding the CP mechanism at 5 GHz: (a) I, (b) II, (c), (d) III, and (e) IV.

3. Understanding The Circular Polarization (CP) and its Analysis Through CEM/GBR Approaches

The responses for CP analysis are given in Figures 5(a)-(e). The primary technique is to examine the behaviour of a CP through the distribution of the surface currents (I). As there are no PCS in antenna-1, it is not possible to create connection with the PGP.

ARTICLE IN PRESS

There is a difference between the vertical surface currents on the monopole arm and induced surface currents on the horizontal spaces of the PGP. Thus, the induced surface currents flow in the opposite direction, as if they were canceling each other. As a result of, a wave of LP is currently forming. When a metallic strip connects with one of the PCS, PCS_L to a PGP in antenna-2, surface currents on the PCS_L and PGP are rearranged so that the currents on the upper edges of the PCS_L & the lower edge of the PGP run in the same direction, resulting in the formation of horizontal surface currents. The viability of CP is dependent on the presence of horizontal and vertical components, referred to as the horizontal and vertical currents shown in Figure 5(a).

Then, the usage of the distribution of the electric field (II) in the analysis of the CP is persuaded. It is possible to achieve LHCP in the +z direction, which is outward in nature, because PCS_L is coupled to PGP by a metallic strip, as electric field vectors rotate in the anticlockwise (ACW) direction, because the phase of the vectors shifts from 0˚ to 90˚ at 5 GHz. As a result of, the presence of an orthogonal change in the pattern of the electric field shows LHCP, demonstrated in Figure 5(b). Further, an examination of the normalized radiation pattern (III) is carried. In Figure 5(c), it shows LHCP. This is because the LHCP gain is greater than the RHCP gain. It is crucial to note that the highest gain at RHCP is 3.39 dBic, whereas the maximum gain for LHCP is 3.58 dBic. Dominancy of CP components is theoretically assessed based on equations (1) & (2) [34], where relative power is considered for LHCP/RHCP & is presented in Figure 5(d), indicating that LHCP is dominating over RHCP. Hence, the investigation into the CP's behavioral explanation was illustrated based on I, II & III. The amplitude & phase responses (IV) in Figure 5(e) are illustrated in a manner that is more effective towards the identification of CP based on the parameters like phase/amplitude. The techniques (I) to (IV) are components of CEM approaches, which are significant & reported for CP analysis. So, it helps to identify the nature of the polarization, either LHCP or RHCP, and then find the dominant CP component in their operating frequency.

$$\vec{E}_{LHCP} = \frac{1}{\sqrt{2}}\left(E_x + jE_y\right) \quad (1)$$

$$\vec{E}_{RHCP} = \frac{1}{\sqrt{2}}\left(E_x - jE_y\right) \quad (2)$$

Continuing with the investigation, gain-bandwidth product relationship (GBR) is a very crucial process [35]. Quite number of equations are utilized to interpret GBR. The equation-(3) of GBR shows that 3-dB bandwidth and 3-dB gain are functions of the criterion:

$$C = F(BW_{3\text{-}dB}, G_{3\text{-}dB}) \quad (3)$$

When it is expressed in the product form, the equation-(3) can be written as:

$$C = BW_{3\text{-}dB} \times G_{3\text{-}dB} \quad (4)$$

Further, it is possible to reframe equation-(4) in the form of a ratio:

$$C = \frac{BW_{3\text{-}dB} \times G_{3\text{-}dB}}{100} \quad (5)$$

At the end, equation-(5) is extended to include the 3-dB bandwidth and 3-dB gain components:

ARTICLE IN PRESS

$$C_1 = \frac{BW_{3\text{-}dB} \times G_{3\text{-}dB(avg)}}{100} \quad (5.1)$$

$$C_2 = \frac{BW_{3\text{-}dB} \times G_{3\text{-}dB(peak)}}{100} \quad (5.2)$$

Use of C_1/C_2 offers an answer to the restrictions that are linked with the methods of comparison. So, comparing the CP antennas to a single characteristic in a practical case is what the traditional technique do. Equation-(5) is a generalized equation for GBR. Table 2 is shown to incorporate the comparison with [14-29]. The evidence shows that the proposed antenna is superior to conventional printed antennas, like (a) increased bandwidth & (b) gain. It offers the CP gain ^{peak} > 5.9 dBic and 3-dB beamwidth > 100° and is able to concentrate the signal with greater precision. When it comes to RF-EH/WPT, requires precise targeting and signal needs to be carried across long distances with little spread or receiving from RF ambient signals, taking into the 5G applications.

Table 2. GBR compares the reported and metamaterial antennas [14-29] (Performance Trade-offs: 10-dB BW > 40%, 3-dB BW >15%, 3-dB gain $^{avg.}$ > 5 dBic, 3-dB gain ^{peak} > 5.9 dBic, FBR > -22 dBic, η > 75%, C_1/C_2 > 1.5. **Nomenclature-** ≠: < Performance Trade-offs, ℘: Not Implemented, ↑: High, ↓: Low, √: > Performance Trade-offs.)

References	**$BW_{3\text{-}dB}$**	**$G_{3\text{-}dB(avg.)}$**	**$G_{3\text{-}dB(peak)}$**	**FBR**	**η**	**C_1**	**C_2**	**AI-Usage**	**Complexity**
[14] 2021	≠	≠	≠	≠	≠	≠	≠	℘	↑
[15] 2015	≠	≠	≠	≠	≠	≠	≠	℘	↑
[16] 2016	≠	≠	≠	≠	≠	≠	≠	℘	↑
[17] 2016	≠	≠	≠	≠	≠	≠	≠	℘	↑
[18] 2018	≠	≠	≠	≠	≠	≠	≠	℘	↑
[19] 2018	≠	≠	≠	≠	≠	≠	≠	℘	↑
[20] 2019	≠	≠	≠	≠	≠	≠	≠	℘	↑
[21] 2020	≠	≠	≠	≠	≠	≠	≠	℘	↑
[22] 2020	≠	≠	≠	≠	≠	≠	≠	℘	↑
[23] 2021	≠	≠	≠	≠	≠	≠	≠	℘	↑
[24] 2021	≠	≠	≠	≠	≠	≠	≠	℘	↑
[25] 2023	≠	≠	≠	≠	≠	≠	≠	℘	↑
[26] 2024	≠	≠	≠	≠	≠	≠	≠	℘	↑
[27] 2025	≠	≠	≠	≠	≠	≠	≠	℘	↑
[28] 2025	≠	≠	≠	≠	≠	≠	≠	℘	↑
[29] 2025	≠	≠	≠	≠	≠	≠	≠	℘	↑
Antenna-1	≠	≠	≠	≠	≠	≠	≠	℘	↑
Antenna-2	≠	≠	≠	≠	≠	≠	≠	℘	↑
Antenna-3	√	√	√	√	√	√	√	√	↓

ARTICLE IN PRESS

ARTICLE IN PRESS

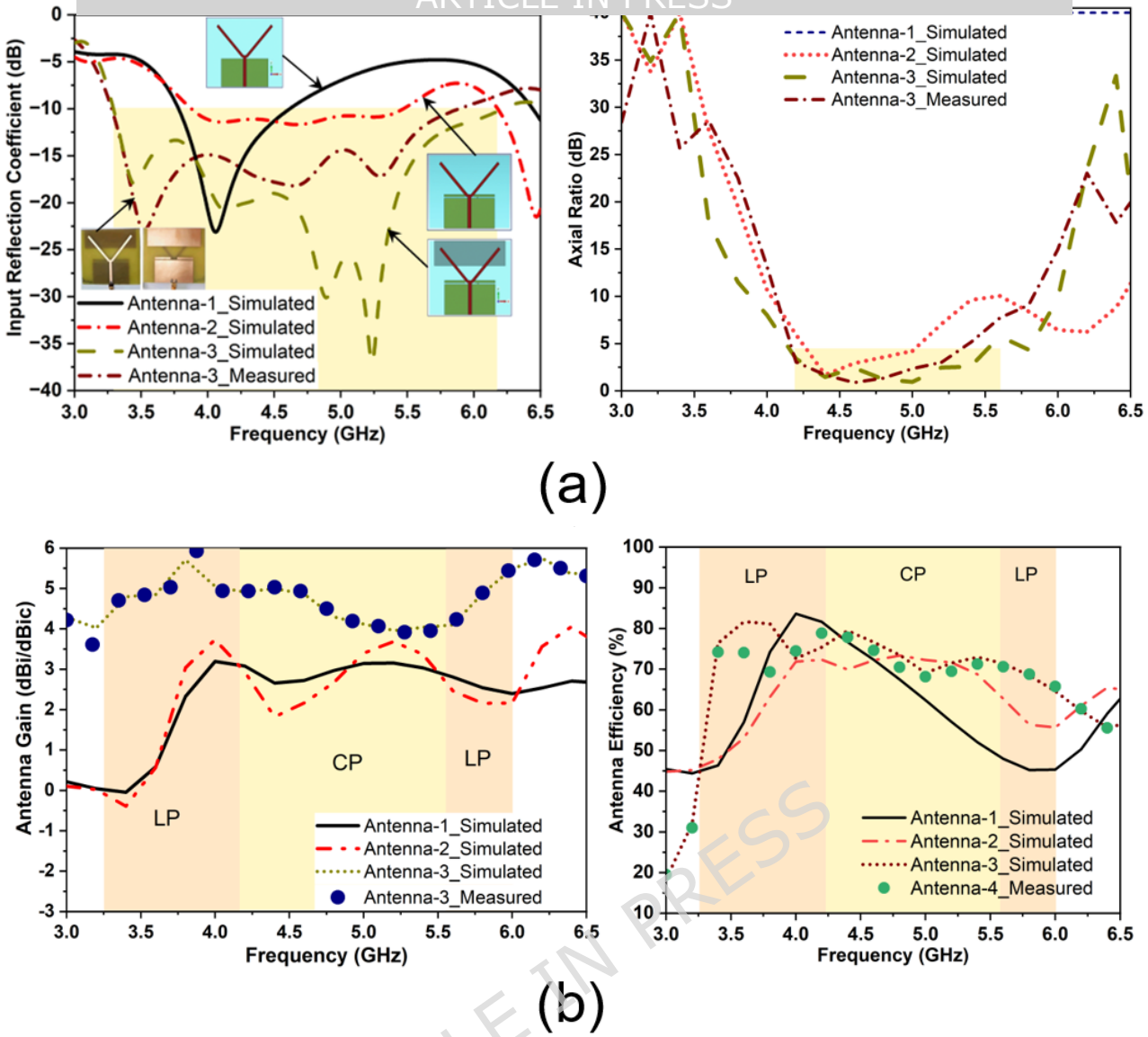

Figure 6. (a) 10-dB, 3-dB bandwidths and (b) Antenna gain & efficiency of the proposed configurations.

ARTICLE IN PRESS

4. Experimental Validation

Figure 1 presents the prototype of proposed antenna that was printed with PCB prototyping mechanism. Table 3 contains the dimensions that are optimized. Presented in Figure 6(a) are the simulated and measured 10-dB BW of 3.03 GHz (3.25-6.28 GHz, 64.58%) and 2.67 GHz (3.25-5.92 GHz, 58.23%). Further, the simulated & measured 3-dB BW of 1.45 GHz (4.04-5.49 GHz, 30.43%) and 1.28 GHz (4.21-5.49 GHz, 26.39%) is shown. In antenna-3, simulated and measured antenna gain, when considered in average in the operating bands, it falls in between 5.25-6 dBic. The antenna efficiency is > 75%, as in Figure 6(b). The boost in gain can be connected with a phase correction, enhanced impedance matching, and decrement of back scattering, where the MTS are serving for the manipulations of waves. It improves the efficiency with which energies are focused in a desired direction, reduces undesirable side lobes, and contributes to the optimization of the spatial distributions of the radiated energy. The normalized radiation pattern at 5 GHz is bi-directional pattern (θ, φ). So, accomplishment of a strong pattern will be the assessment of the efficiency of the transmission and reception of EM waves. To be specific, it has shown impact on the ability to concentrate on these RF signals arriving from the front side, simultaneously minimizing the interference coming from a rear side. MTS provides reduction in interference by shaping the waves, filtering frequencies, & beam pattern. So, one of the qualities that make them beneficial for enhancing communication system in

ARTICLE IN PRESS

sophisticated circumstances is the dynamic adjustments & fine tuning capabilities that they provide. Deployment of the SADEA-tuned MTS layer as parasitic patch was responsible for the achievement of performance trade-offs. A number of features that are connected with radiation patterns are observed in Figures 7(a) and (b), respectively including the attainment of optimum front-to-back ratio i.e., FBR. Thus, attainment of stronger FBR will be the evaluation regarding the effectiveness of the transmission and reception of EM waves for RF energy harvesting applications.

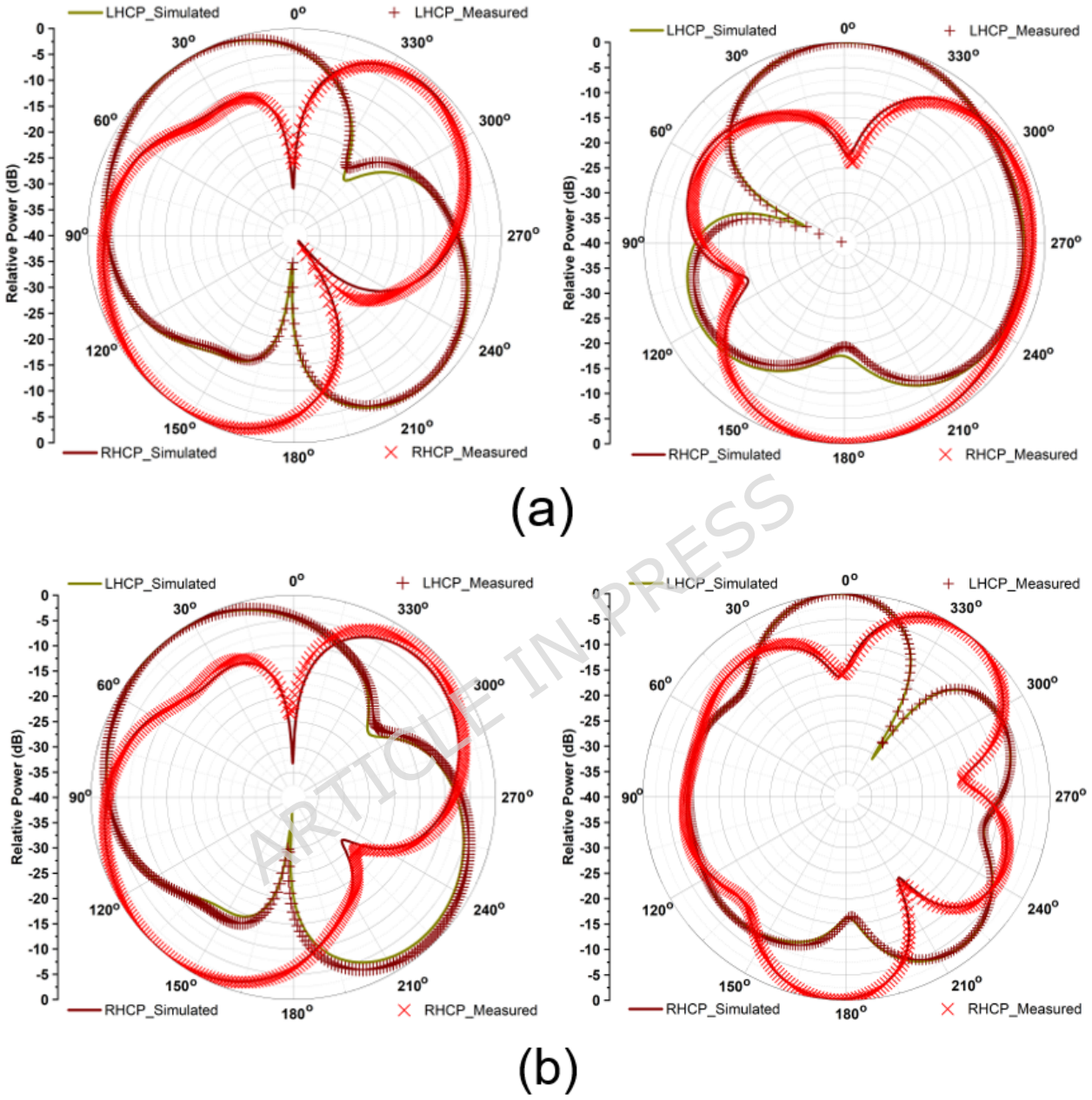

Figure 7. Far-field radiation pattern of antenna-3 (final stage) at (a) f=4.5 GHz and (b) f=5 GHz.

In order to conduct a more in-depth analysis, it is essential to take into consideration the fact that equation-(6) [36] is responsible for determining the effective gap ($h_{air\text{-}gap}$) that exists between the radiator & SADEA-driven MTS layer. It encompasses the thickness of the substrate (h_{sub}), relative permittivity of the substrate (ε_r), and wavelength at which it operates (λ_o). The theoretical $h_{air\text{-}gap}$ is computed to be at 1.76 mm, while the simulated $h_{air\text{-}gap}$ is 1.635 mm. So, this formulation is utilized for deploying these MTS reflectors. It is accomplished by approximating the $h_{air\text{-}gap}$ through the usage of the given analytical approach:

$$h_{air\text{-}gap} = 0.085\lambda_0 - h_{sub}\sqrt{\varepsilon_r} \quad (6)$$

ARTICLE IN PRESS

Figure 8(a) presents the MTS simulation with the consideration of periodic boundary conditions. The reflection and transmission characteristics show the dominant reflection occurs at f=4.5 GHz with a consistent (S_{11}, S_{22}) dB responses, while the transmission parameters (S_{12}=S_{21}) witness an out-of-band characteristic at the desired band, illustrated in Figure 8(b). While doing the individual analysis, it is observed that harmonically balanced resonant parameters stabilize the series capacitances with the shunt inductances. This response stabilization is attained by series capacitance in between the shunt inductances [37, 38]. The smooth responses of S11 & S22 validate the proposed MTS layer as a parasitic patch to act like a metamaterial configuration. More information on it can be retrieved if we analyze it through the consideration of refractive index properties, where it acts as DNG material, as shown in Figure 8(c). Thus, the MTS layer, which is used as a parasitic patch in our proposed design, resulted in the significant improvement of impedance and axial bandwidths, along with a considerable enhancement of gain, taking into consideration of performance trade-offs from an application perspective.

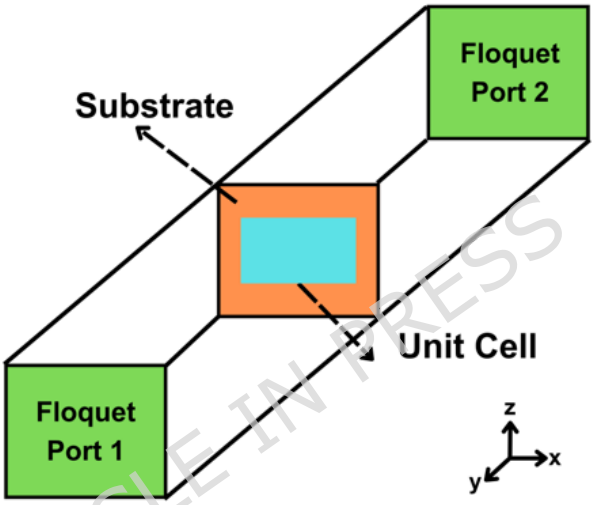

(a)

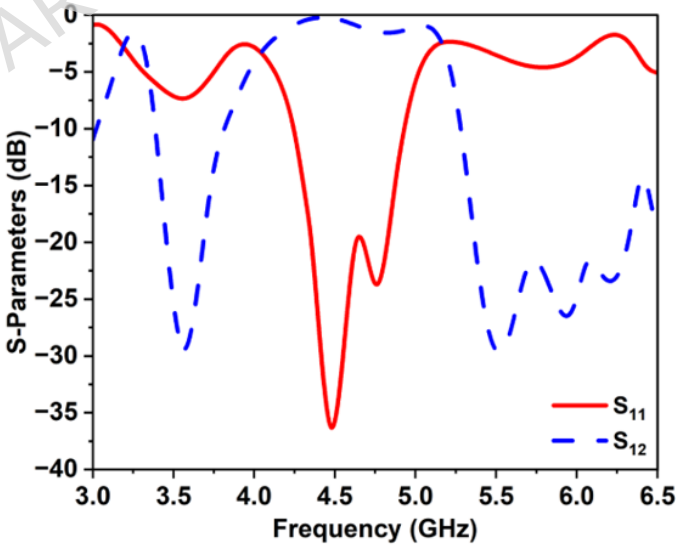

(b)

ARTICLE IN PRESS

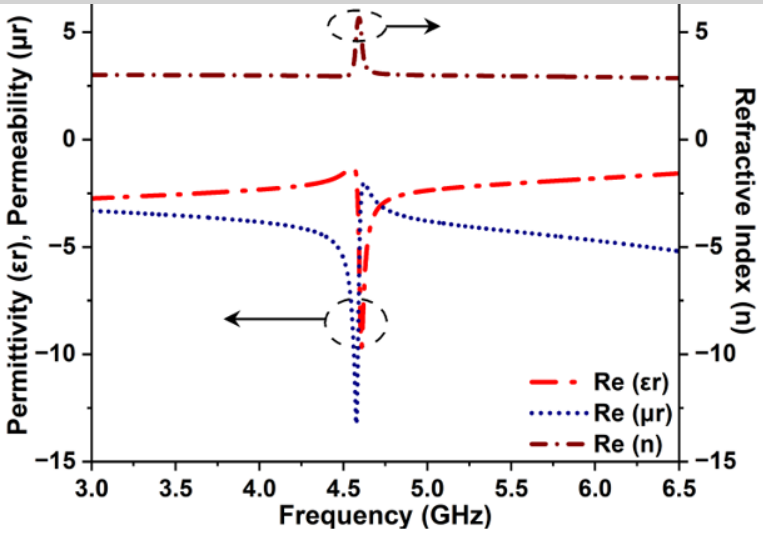

(c)

Figure 8. (a) Excitation, (b) Transmission and reflection characteristics, and (c) Refractive index of the MTS as a parasitic patch.

For antenna-3, the equivalent circuit model is presented in Figure 9 with the lumped R-L-C network by using an ADS solver. The antenna witnesses parallel harmonics between real and imaginary resonances. The discrete resonances are fundamentally coupled by adding R-C-L in a parallel mode. So, the circuit components (R1, C1, L1),.....(R3, C3, L3) denote antenna-3, which is capacitively coupled through C11, C22, C33, meant to stabilize the harmonics. It is excited by port impedance of 50 Ω, and its feeding mechanism is coupled via resistive-inductive elements (Rp, Lp) separated by capacitance (Cg). The MTS as a parasitic patch is modeled as LC-periodic elements: inductances in parallel & capacitance in series for attaining performance trade-offs. The required S11 outcomes for the equivalent circuit model are presented in Figure 10. Prior to it, the values of all the R-C-L components are given in the ranges of:

- R1= (60.76-to-63.82) Ω || C1= (0.041-0.045) pF || L1= (11.43-11.45) nH
- C11=(0.022-to-0.024) pF
- R2= (61.32-65.24) Ω || C2= (0.115-0.119) pF || L2= (9.81-9.85) nH
- C22=C33=(0.007-to-0.008) pF
- R3= (100.5-100.9) Ω || C3= (0.06-0.09) pF || L3=(8.15-to-8.19) nH,
- Rp=50Ω || Cg=1pF=Ca1=Ca2=Ca3...=Ca6=Cg1=Cg2=Cg3=...=Cg6
- Lp=La1=La2=La3...=La6=Lb1=Lb2=Lb3....=Lb6=1nH= Lc1=Lc2=Lc3=...=Lc6 & Port=50-Ω.

(**Note:** All the values that are considered in this equivalent circuit model - ECM are required to be tuned for getting its operation in the desired impedance bandwidth range).

ARTICLE IN PRESS

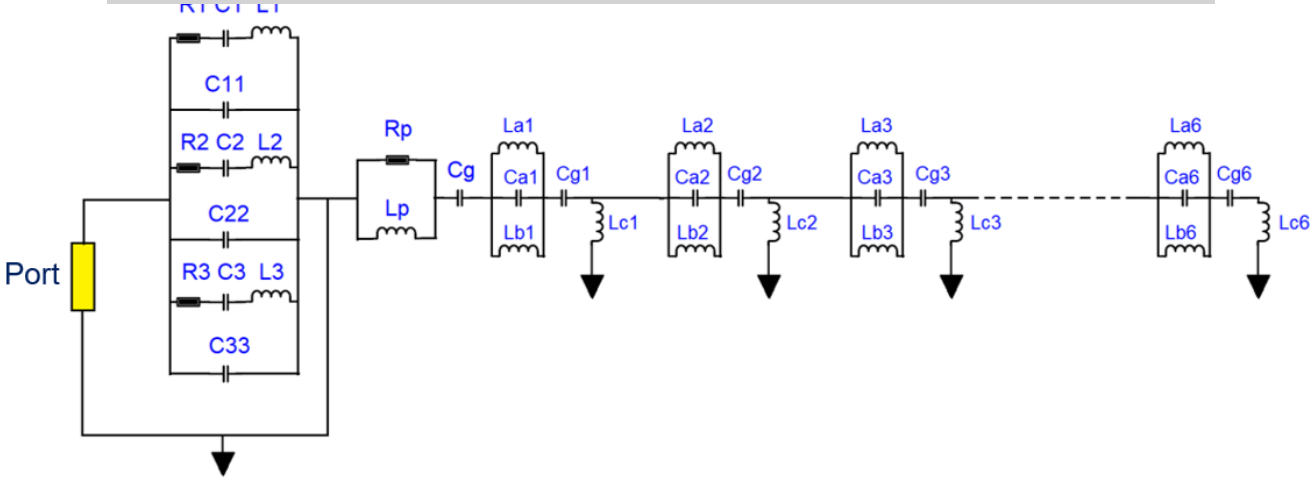

Figure 9. ECM of the proposed antenna configuration (antenna-3).

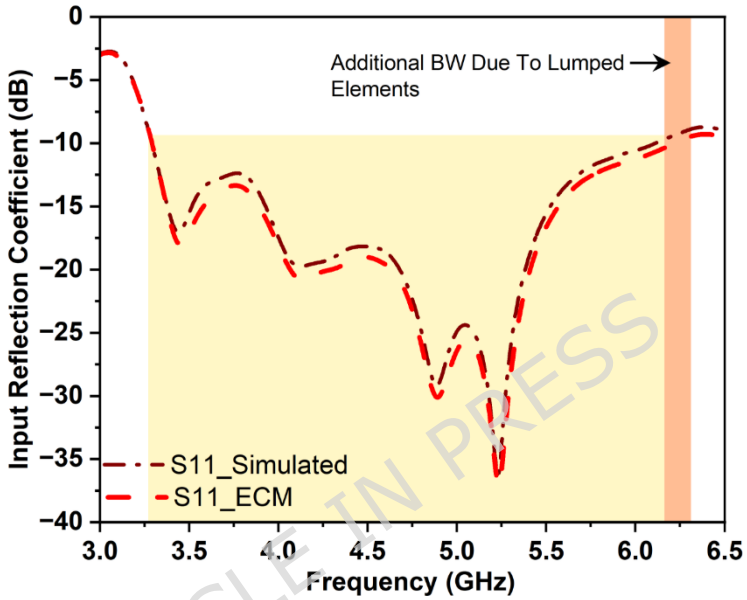

Figure 10. S11 outcomes depicting a bandwidth from 3.26 to 6.32 GHz obtained after implementing the ECM for antenna-3.

From the Figures 9 and 10, it is observed that the equivalent circuit model (ECM) makes it easier to understand how an antenna behaves by modeling it with RLC components. These elements show how energy is stored & lost within, helping explain how resonance, impedance matching, & bandwidth are controlled. The inductance and capacitance determine the resonant frequency, while the resistance reflects radiation and material losses, influencing efficiency and input impedance. Overall, the ECM provides a clear and practical way to connect physical design changes with the antenna's performance [39, 40].

In this investigation, the CST Microwave Studio (CST-MWS) is used as the full-wave electromagnetic solver, KEYSIGHT ADS circuit solver is used for designing the equivalent circuit diagram, and MATLAB is utilized for executing the AI-tuned optimization method, i.e., SADEA. To sum up, the final schematic and its requisite dimensions are presented in Figure 11(a) and Table 3. Continuing to the next part of the investigation, we look at how the antenna-3 works in the sub-6 GHz 5G bands; the analysis and simulation for RF energy harvesting will be carried out based on the CRLH matching GVD rectifier circuit given in Figure 9(b). Its outcomes, such as V_{out} and η_o, are reported in Figure 12, compared with the reported works in [41-50] belonging to the same field of interest.

ARTICLE IN PRESS

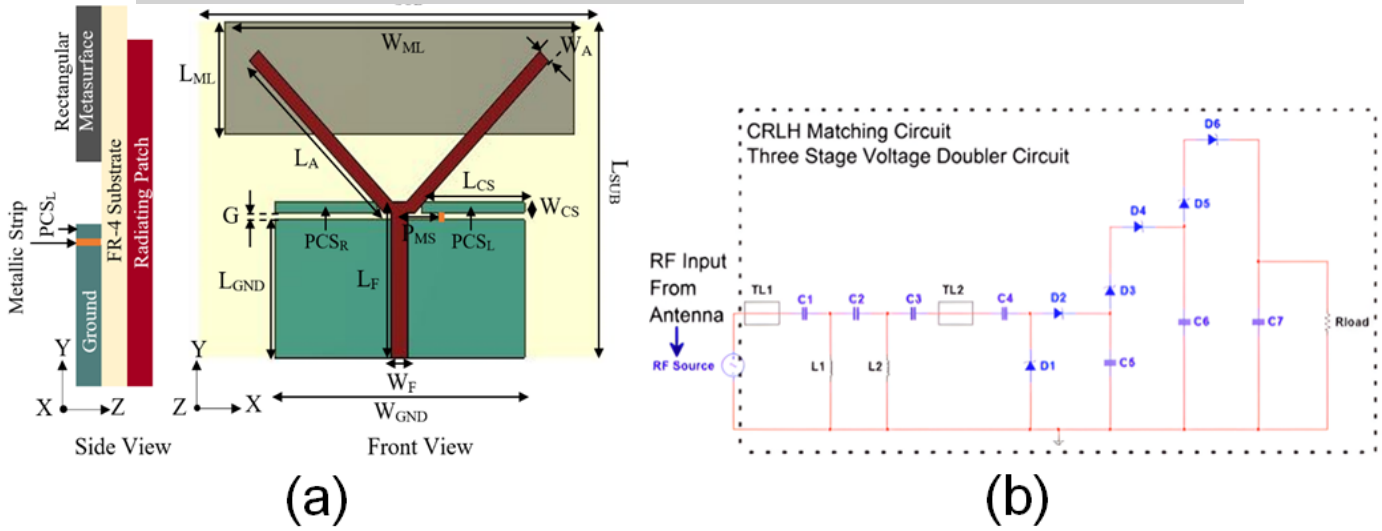

Figure 11. Final schematics: (a) Antenna-3 (final stage) and (b) CRLH matching GVD rectifier circuit.

Table 3. Final dimensions of the antenna-3 and CRLH matching rectifier circuit used in our investigation.

Antenna-3		Rectifier Circuit	
Parameters	**Values**	**Parameters**	**Values**
W_{SUB}	80 mm	L1	2.1 nH
L_{SUB}	60 mm	L2	
W_{ML}	70 mm	C1	1.68 pF
L_{ML}	20 mm	C2	0.84 pF
W_A	2.5 mm	C3	1.68 pF
L_A	38 mm	C4	100 pF
W_{CS}	1.16 mm	C5	
L_{CS}	20.6 mm	C6	
PCS_L	20.6 mm	C7	
PCS_R	20.6 mm	D1	SMS 7630
P_{MS}	3.5 mm	D2	
W_F	3.5 mm	D3	
L_F	27 mm	D4	
W_{GND}	50 mm	D5	
L_{GND}	25 mm	D6	
G	1.1 mm	D7	
Substrate	FR-4, 1.6 mm	Rload	2.2 kΩ

5. Simulation Perspective of RF Energy Harvesting/Wireless Energy Harvesting Application

RF energy harvesting requires the conversion of RF signals into a DC output. So, this is accomplished by the utilization of a wideband rectifier circuit (GVD) & an impedance matching network (IMN) that is coupled to the proposed antenna (antenna-3). The success of the entire system is dependent on the degrees of these three components. Coming to our objective, develop the system that is capable of meeting the ever-increasing power requirements of multifunctional electronic components, provided that antennas are able to achieve balance in their performance before being incorporated into the RF circuits. It should be capable of supplying DC power to the sensors that are found in the LPEDs, like wearables and medical & healthcare plug-in kits. These sensors

ARTICLE IN PRESS

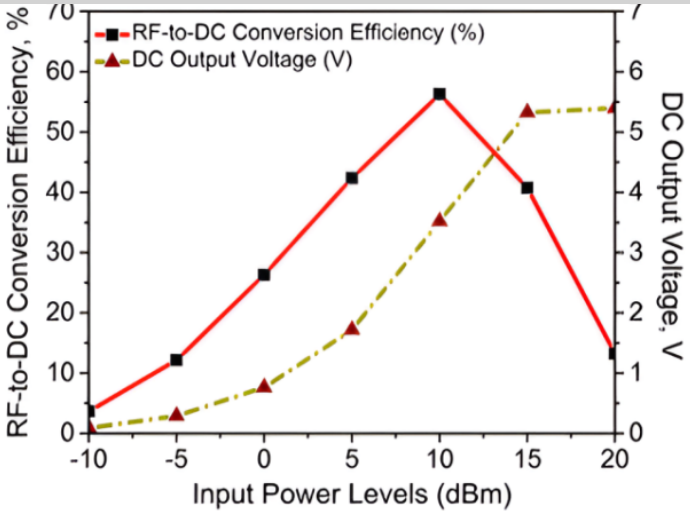

Figure 12. RF energy harvesting outcomes for the proposed antenna (antenna-3) at f=5 GHz.

Table 4. Comparative study of the outcomes attained at various stages of the proposed antenna. (Performance Trade-offs*: 10-dB BW > 45%, 3-dB BW >15%, & CP gain $^{avg.}$ > 5 dBic is taken into consideration from an application perspective. **Nomenclature-** ≠: < Performance Trade-offs √: > Performance Trade-offs.).

Parameters	**Antenna-1**	**Antenna-2**	**Antenna-3**	**Improvement By a Factor**
10-dB BW (%)	18.86%	12.59%	64.58%	5.12 Times
3-dB BW (%)	≠	11.46%	30.43%	2.65 Times
CP Antenna Gain $_{Avg.}$	≠	2.35 dBic	5.28 dBic	2.24 Times
Trade-offs*	Not Attained	Not Attained	Attained	×
P_{in}	≠	10 dBm	10 dBm	×
V_{out} @ 5 GHz	≠	1.08 V	3.58 V	3.31 Times
η_o @ 5 GHz	≠	28%	58%	1.96 Times

Table 5. Comparative study of the RF energy harvesting outcomes attained for the antenna-3. (Performance Trade-offs*: V_{out} > 1.5 V and η_o > 45% is considered w.r.t. [41-50], **Nomenclature-**≠: < Performance Trade-offs √: > Performance Trade-offs.).

References	**P_{in} (Input Power Levels)**	**V_{out} (DC Output Voltage)**	**η_o (RF-to-DC Conversion Efficiency)**
[41] ^{2019}	5 dBm	≠	≠
[42] ^{2019}	5 dBm	≠	≠
[43] ^{2020}	5 dBm	≠	≠
[44] ^{2022}	5 dBm	≠	≠
[45] ^{2023}	5 dBm	√	√
[46] ^{2023}	5 dBm	≠	≠
[47] ^{2024}	×	≠	≠
[48] ^{2024}	5 dBm	≠	≠
[49] ^{2024}	5 dBm	≠	≠
[50] ^{2025}	5 dBm	≠	≠
Antenna-3	**5 dBm**	**1.58 V (√)**	**~47% (√)**

require V_{out} ranging from 2.45-5.5 V in order to function. Hence, to incorporate it in a controlled environment, a 3-stage GVD circuit built with a CRLH-matching rectifier circuit is designed & integrated with the antenna-3, shown in Figure 11(b). For this

ARTICLE IN PRESS

purpose, it is explored for the P_{in} that spans from -5 to +20 dBm, where the V_{out} witnesses a maximum of 3.58 V and η_0 > 55% at 10 dBm. This is achieved by maintaining a load resistance of 2.2 kΩ at 5 GHz. A comparison has been made with the recent works reported in [41-50], where the desired outcomes (V_{out}, η_0) attained through a simulation on the ADS platform are superior in a quantitative way. A comprehensive analysis of the results obtained is given in Figure 12 and Tables 4 & 5. Commencing the next part of the investigation, our future scope is to improve η_0 to > 70% in the sub-6 GHz 5G band that is calculated by using the equation-(7) [11].

$$h_0 = \frac{P_{load}}{P_{incident}} = \frac{V_{out}^2}{P_{in} \times R_{load}} \times 100\% \quad (7)$$

Prior to the simulation, theoretical insights about the proposed rectifier model are also investigated. Here, each individual stage with its dedicated GVD configuration is considered as the single battery having open circuit output voltage ($V_{o.c.}$), internal resistance (R_{int}), and load resistance (R_{load}). Henceforth, the output voltage (V_{out}) can be expressed in equation-(8) [11] for n-stages as follows:

$$V_{out} = \frac{nV_{o.c.}}{nR_{\text{int}} + R_{load}} \times R_{load} \quad (8)$$

6. Conclusion and its Future Scope

An investigation into a CP printed monopole antenna loaded with the SADEA-tuned MTS layer as a parasitic patch is given in this paper. Due to this, it is feasible to attain an expanded 10-dB BW and 3-dB BW, with CP gain $^{\text{peak}}$ > 5.9 dBic and antenna efficiency > 75% in their desired bands. In addition to the insights about CP, a complete analogy is presented for providing a solution to the problem of assessing CP by using CEM/GBR. It is also observed that, by lowering the need for complex simulation, the AI-driven SADEA method witnesses an effective way to optimize antenna designs while preserving the strength of DEs for reducing the complexity. In a scenario where resources and time are constrained, this optimization is extremely useful for attainment of performance trade-offs from an application perspective. As a result of it, it is well acclaimed that the landscape of next-generation wireless communication is in an era of experiencing the paradigm shift, in accordance with the increasing needs of applications in the upcoming scopes in the likes of RIS, IRS, UAV, V2V, etc. At last, our research mainly concentrates on DAVI, encompassing the stages such as design, analysis, validation, and implementation, enhancing its overall effectiveness. It is assumed that sustainable technology will depend on effective antennas as the wireless communication networks expand and the demand for the low-power, energy-efficient devices rises by following the notions of RF energy harvesting (RF-EH) in the sub-6 GHz bands.

References

1. Dai, M.; Sun, G.; Yu, H.; Wang, S.; & Niyato, D. User association and channel allocation in 5G mobile asymmetric multi-band heterogeneous networks. *IEEE Trans. Mob. Comput.* **24**, 3092-3109 (2025).
2. Zhao, Z. *et al*. Design and analysis of a 22.6-to-73.9 GHz low-noise amplifier for 5G NR FR2 and NR-U multiband/multistandard communications. *IEEE J. Solid-State Circuits*. **60**, 3189-3201 (2025).
3. Luo, H.; Sun, G.; Chi, C. *et al*. Convergence of symbiotic communications and blockchain for sustainable and trustworthy 6G wireless networks. *IEEE Wirel. Commun*. **32**, 18-25 (2025).

ARTICLE IN PRESS

4. Zhang, Y. et al. Design and analysis of a compact 0.13-μm SiGe power amplifier with 29.2-dBm P SAT and 44.4% PAE for FR3 5G-advanced/6G beamforming systems. *IEEE J. Solid-State Circuits*, Early Access, (2025).
5. Sun, J.; Zhou, Sha.; & Lin, Q. A high-precision and fast modeling method for amplifiers. *Int J. Numer. Model*. **38**, e70051 (2025).
6. Zou, X. -J. *et al*. Miniaturized low-profile ultrawideband antipodal Vivaldi antenna array loaded with edge techniques. *IEEE Trans. Antennas Propag.* **74**, 1156-1161 (2026).
7. Hussain, N.; Naqvi S. *et al*. A metasurface-based wideband bidirectional same-sense circularly polarized antenna. *Int. J. RF Microw. Comput Aided Eng*. **30**, e22262 (2020).
8. Hussain, N. *et al*. A broadband circularly polarized Fabry-Perot resonant antenna using a single-layered PRS for 5G MIMO applications. *IEEE Access*. **7**, 42897-42907 (2019).
9. Tran, H. H.; Hussain, N.; & Le, T. T. Low-profile wideband circularly polarized MIMO antenna with polarization diversity for WLAN applications. *AEU - Int. J. Electron*. **108**, 172-180 (2019).
10. Hussain, N. *et al*. Metasurface-based single-layer wideband circularly polarized MIMO antenna for 5G millimeter-wave systems. *IEEE Access*. **8**, 130293-130304 (2020).
11. Behera, B. R.; Meher, P. R.; & Mishra S. K. Metasurface superstrate inspired printed monopole antenna for RF energy harvesting application. *Prog. Electromagn. Res. C*. **110**, 119-133 (2021).
12. Meher, P. R.; Behera, B. R.; & Mishra S. K. A compact circularly polarized cubic DRA with unit-step fe-
-ed for Bluetooth/ISM/Wi-Fi/Wi-MAX applications. *AEU - Int. J. Electron*. **128**, 153521 (2021).
13. Divakaran, S.; Krishna, D. D.; & Nasimuddin, N. RF energy harvesting systems: An overview and design
issues. *Int. J. RF Microw. Comput Aided Eng*. **30**, e22148 (2019).
14. Elahi, M. *et al*. Circularly polarized dielectric resonator antenna with two annular vias. *IEEE Access*. **9**,
41123-41128 (2021).
15. Yang, W.; Che, W.; Jin, H.; Feng, W.; & Xue, Q. A polarization-reconfigurable dipole antenna using polarization rotation AMC structure. *IEEE Trans. Antenn. Propag*. **63**, 5305-5315 (2015).
16. Yue, T.; Jiang, Z. H.; & Werner, D. H. Compact, wideband antennas enabled by interdigitated capacitor-loaded metasurfaces. *IEEE Trans. Antenn. Propag*. **64**, 1595-1606 (2016).
17. Wu, Z.; Li, L.; Li, Y.; & Chen, X. Metasurface superstrate antenna with wideband circular polarization for the satellite communication application. *IEEE Antenn. Wirel. Propag. Lett*. **15**, 374-377 (2016).
18. Chen, Q.; Zhang, H. *et al.* Wideband and low axial ratio circularly polarized antenna using AMC-based structure polarization rotation reflective surface. *Int. J. Microw. Wirel. Technol*. **10**, 1058-1064 (2018).
19. Lin, W. *et al*. Reconfigurable, wideband, low profile, circularly polarized antenna and array enabled by artificial magnetic conductor ground. *IEEE Trans. Antenn. Propag*. **66**, 1564-1569 (2018).

ARTICLE IN PRESS

ARTICLE IN PRESS

20. Kumar, A.; Thanikanti, S. N.; & Chaudhary, R. Improvements in Wi-MAX reception: A new dual-mode wideband circularly polarized dielectric resonator antenna. *IEEE Antenn. Propag. Mag*. **61**, 41-49 (2019).
21. Ameen, M.; & Chaudhary, R. Dual-layer and dual-polarized metamaterial inspired antenna using circular-complementary split ring resonator mushroom and metasurface for wireless applications. *AEU - Int. J. Electron.* **113**, 1529771 (2020).
22. Rajanna, P.; Rudramuni, K.; & Kandasamy, K. Characteristic mode-based compact circularly polarized metasurface antenna for in-band RCS reduction. *Int. J. Microw. Wirel. Technol*. **12**, 131-137 (2020).
23. Ameen, M.; & Chaudhary, R. Metamaterial circularly polarized antennas: Integrating an epsilon negative transmission line and single split ring-type resonator. *IEEE Antenn. Propag. Mag*. **63**, 60-77 (2021).
24. Chen, A.; Ning, X. A pattern and polarization reconfigurable antenna with metasurface. *Int. J. RF Microw. Comput Aided Eng*. **31**, e22312 (2021).
25. Liu, T. *et al*. A broadband circularly polarized antenna based on transparent conformal metasurface. *IEEE Antenn. Propag. Mag*. **22**, 3197-3201 (2023).
26. Parasher, R.; Yadav, D.; & Saharia, S. Metamaterial-based octagonal ring penta-band antenna for sub-6 GHz 5G, WLAN, and WiMAX wireless applications. *Prog. Electromagn. Res. B*. **104**, 109-129 (2024).
27. Khadar, S.K.; & Sahu, S. A tri-band CP MIMO antenna influenced by metasurface for next generation wireless communication. *J. Electromagn. Waves Appl*. **39**, 1794-1823 (2025).
28. Bose, M. & Karuppiah, V. Metamaterial inspired superstrate loaded miniaturized quad port MIMO ante- -nna for 5G C-band applications. *Opt. Commun*. **574**, 131123 (2025).
29. Singh, S.K. *et al*. A compact triple-band CPW-fed antenna laminated on FR-4 dielectric substrate material for diverse wireless applications. *Curr. Appl. Phys*. **71**, 27-36 (2025).
30. Liu, B. *et al*. An efficient method for antenna design optimization based on evolutionary computation and machine learning techniques. *IEEE Trans. Antenn. Propag*. **62**, 7-18 (2013).
31. Liu, B.; Koziel, S.; & Ali, N. SADEA-II: A generalized method for efficient global optimization of antenna design. *J. Comput. Des. Eng*. **4**, 86-97 (2016).
32. Liu, B. *et al*. An efficient method for complex antenna design based on a self-adaptive surrogate model-assisted optimization technique. *IEEE Trans. Antenn. Propag*. **69**, 2302-2315 (2021).
33. Liu, Y. *et al*. An efficient method for antenna design based on a self-adaptive Bayesian neural network-assisted global optimization technique. *IEEE Trans. Antenn. Propag*. **70**, 11375-11388 (2022).
34. Toh, B. Y.; Cahill, R.; & Fusco, V. F. Understanding and measuring circular polarization. *IEEE Trans. Educ.* **46**, 313-318 (2003).
35. Kirov, G. S. Evaluation of the frequency bandwidth and gain properties of antennas: Characteristics of circularly polarized microstrip antennas. *IEEE Antenn. Propag. Mag.* **62**, 74-82 (2020).
36. Abbas Awan, W. *et al*. Intelligent metasurface based antenna with pattern and beam reconfigurability for internet of things applications. *Alex. Eng. J.* **92**, 50-62 (2024).

ARTICLE IN PRESS

ARTICLE IN PRESS

37. Mohanty, A. *et al*. Investigation of a dual-layer metasurface inspired fractal antenna with dual-polarized/-modes for 4G/5G applications. *Electronics*. **11**, 2371 (2022).
38. A Mohanty, A. *et al*. Investigation of a miniaturized four-element antenna integrated with dipole elements
and meta-couplers for 5G applications. *Sensors*. **22**, 5355 (2022).
39. Abbas Awan, W; Abbas, A. *et al*. Compact and directional dual band antenna with low mutual coupling MIMO configuration for mm-wave communication. *Results in Engineering*. **26**, 105457 (2025).
40. Hussain, M.; Abbas Awan, W.; Zahra, H. *et al.* Design and characterization of multiwall carbon nanotube/ polydimethylsiloxane composite MIMO antenna for wearable and vehicular applications. *Sci Rep*. **15**, 27925 (2025).
41. Jie, A.; Nasimuddin; Karim, M. F.; & Chandrasekaran, K. T. A wide-angle circularly polarized tapered-slit-patch antenna with the compact rectifier for energy-harvesting systems. *IEEE Antenn. Propag. Mag*. **69**, 94-111 (2019).
42. Noor, M. F. *et al*. A. Dual-band aperture-coupled rectenna for radio frequency energy harvesting. *Int. J. RF Microw. Comput Aided Eng*. **29**, e21651 (2019).
43. Chandrasekaran, K. *et al*. Compact dual-band metamaterial-based high-efficiency rectenna: Application for ambient electromagnetic energy harvesting. *IEEE Antenn. Propag. Mag*. **62**, 18-29 (2020).
44. Surender, D. *et al*. Circularly polarized DR-rectenna for the 5G and Wi-Fi bands RF energy harvesting in smart city applications. *IETE Tech Rev*. **39**, 880-893 (2022).
45. Bougas, I. D. *et al*. Dual-band rectifier circuit design for IoT communication in 5G systems. *Technologies.* **11**, 34 (2023).
46. Yue, Z.; Xu, X. *et al*. Design of efficient and compact ultrawideband rectifier for sub-6 GHz WPT/EH. *IEEE Microw. Wirel. Technol. Lett*. **33**, 1490-1493 (2023).
47. Kong, Y.; Bai, X. *et al*. High-efficiency 5G-band rectifier with impedance dispersion compensation netw--ork. *Electronics*. **13**, 3105 (2024).
48. Gyawali, B.; Aboualalaa, M.; Barakat, A.; & Pokharel, R. Design of the miniaturized sub-6 GHz rectifier with self-impedance matching technique. *IEEE Trans. Circuits Syst. I: Regul. Pap*. **71**, 3413-3422 (2024).
49. Halimi, Md. A., Khan, T., Kishk, A. A.; & Antar, Y. Efficient rectifier circuit operating at N78 and N79 sub-6 GHz 5G bands for microwave energy-harvesting and power transfer applications. *Int. J. Microw. Wirel. Technol*. **16**, 75-82 (2024).
50. Bairappaka, S.; Ghosh, A. *et al*. A dual-band dual-polarized rectenna for efficient RF energy harvesting in battery-less IoT devices with broad power range. *Int. J. Commun. Syst*. **38**, e6103 (2025).

Acknowledgements

The authors would like to thank the support of Sejong University Seoul, South Korea for helping us in carrying out the research work.

Funding

The research work was funded by Sejong University, Korea.

Author Contributions

Concepts: Bikash Ranjan Behera and Harikrishna Paik.; **Methodology:** Bikash Ranjan Behera, Harikrishna Paik, J. Arun Kumar, Mohammed H. Alsharif, & Sabri Saeed; **Writing-Original Draft Preparation**: Bikash Ranjan Behera, Harikrishna Paik, J. Arun Kumar, Mohammed H. Alsharif, & Khalid Yahya; **Writing-Final Review and Editing**: Bikash Ranjan Behera, Mohammed H. Alsharif, Sabri Saeed, & Khalid

ARTICLE IN PRESS

Yahya; **Project Administration:** Mohammed H. Alsharif & Khalid Yahya; **Funding Acquisition:** Mohammed H. Alsharif, Sabri Saeed, & Khalid Yahya.

Data Availability Statement

The datasets used and analyzed during the research are available from the corresponding author on the request.

Human and Animal Rights

It does not contain any studies with human participants or animals performed by any of the authors.

Competing Interest

The authors declare that there is no conflict of interest.

ARTICLE IN PRESS